

Direct and charge-transfer scattering of keV-energy H^+ and He^+ projectiles from rare-gas atoms to obtain small-angle absolute differential cross sections

L. K. Johnson, R. S. Gao, C. L. Hakes, K. A. Smith, and R. F. Stebbings

Department of Physics, Department of Space Physics and Astronomy, and Rice Quantum Institute, Rice University, P.O. Box 1892, Houston, Texas 77251

(Received 30 May 1989)

Measurements of absolute differential cross sections for direct and charge-transfer scattering of H^+ and He^+ by the rare gases have been made. Direct scattering cross sections are reported at 1.5 keV for collisions of H^+ and He^+ with Ne, Ar, Kr, and Xe over the laboratory angular range 0.03° – 1.0° . Charge-transfer cross sections are reported for the laboratory scattering angles below 1.0° for H^+ -Ar, Kr at 0.5, 1.5, and 5.0 keV, for H^+ -Xe at 5.0 keV, and for He^+ -Ne at 1.5 keV. The data exhibit a wealth of structure over the experimental angular range, and cross sections have been integrated over angle to provide absolute integral cross sections.

I. INTRODUCTION

Differential scattering in asymmetric ion–rare-gas collisions has been the subject of considerable experimental effort. In particular, differential scattering for He^+ –rare-gas processes has been studied in the energy range 10–600 eV by Aberth, Lorents, Smith, and others associated with the Stanford Research Institute^{1,2} (SRI), and for H^+ - and He^+ -rare gas from 60–3000 eV by Barat, Abignoli, Benoit, Baudon, Kubach, and others associated with the Centre National de la Recherche Scientifique (CNRS) at Orsay, France.^{3–7} The SRI group measured absolute-differential cross sections over the angular range 1° – 30° for He^+ -Ne and He^+ -Ar, while the CNRS group measured relative differential cross sections over the range 0.5° – 20° . Both groups measured the energy loss of scattered projectiles and compared structure in the data with *ab initio* calculations, semiclassical scattering theory, or “curve-crossing” models.⁸

Previous papers originating in this laboratory described techniques for measuring keV-energy absolute-differential cross sections at very small angles ($0.05^\circ \leq \theta \leq 1^\circ$) with high angular resolution (0.02° at the smallest angles). Differential cross sections for scattering of H and He projectiles by a variety of rare-gas and diatomic molecular targets were reported,⁹ as were direct scattering and charge-transfer data for collisions of H^+ and He^+ with He.^{10,11} Differential cross sections obtained at these small angles contain information that permitted evaluation of calculated or proposed interaction potentials.

In this paper, differential cross sections for direct and charge-transfer scattering of H^+ and He^+ projectiles from Ne, Ar, Kr, and Xe targets are reported. The term “direct” scattering expresses the fact that the detected particle’s charge is the same as the projectile’s; “elastic” scattering is reserved for direct events in which no electron excitation occurs. Theoretical interpretations of the data are not attempted; instead, emphasis is placed on presenting a spectrum of experimental results. In addition,

integration of the differential cross section over angle has been performed to provide integral cross sections which, since the scattering is highly concentrated at small angles, contain the bulk of the total cross sections.

II. APPARATUS AND EXPERIMENTAL METHOD

The apparatus, shown in Fig. 1, has been described in previous publications.^{10–12} Ions emerging from the source are accelerated to the desired energy and focused electrostatically. The resulting ion beam is momentum analyzed by two sector magnets and the mass-selected beam of H^+ or He^+ passes through a collimating aperture before arriving at the target cell (TC), which is about 0.4 cm long. The entrance aperture of the TC ($30 \mu\text{m}$ diameter) and the collimating aperture ($20 \mu\text{m}$ diameter) are separated by 49 cm, limiting the angular divergence in the beam to 0.003° . A 4.0-cm-diam position-sensitive detector (PSD) located 109 cm from the TC monitors both the primary beam and fast collision products. An electrostatic field may be established between deflection plates (DP) to prevent primary and scattered ions from striking the detector. An LSI 11/2 microcomputer sorts the arrival coordinates of each detected particle into bins in a 90×90 array; the minimum physical bin size for the present experiments is $109 \times 109 \mu\text{m}^2$. Care is taken to

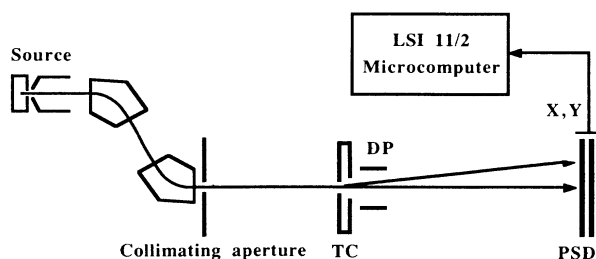


FIG. 1. Schematic of the apparatus.

measure this bin size accurately and to determine the position-finding accuracy of the PSD system. Background chamber pressure is about 2×10^{-7} torr, while the TC pressure is typically a few millitorr; thin target conditions thus prevail, and so differential cross sections are given by

$$\frac{d\sigma(\theta)}{d\Omega} = \frac{\Delta S(\theta)}{SnL\Delta\Omega}, \quad (1)$$

where S is the primary ion beam flux, $\Delta S(\theta)$ is the flux scattered at angle θ into a solid angle $\Delta\Omega$, n is the target number density (obtained from the TC gas pressure), and L is the TC length.

During charge-transfer measurements, ions emerging from the TC are deflected away from the PSD so that only neutral collision products are detected. The primary beam is intermittently returned to the detector to monitor the primary beam flux. The 90×90 PSD data array is partitioned into a set of narrow rings centered at the primary beam position, taking advantage of the azimuthal symmetry of the scattering pattern. The centermost ring (actually a disk) contains signal due to charge-transfer scattering at 0° ; the smallest angle presented for differential cross sections is the mean angle of this ring. Differential cross sections are obtained according to Eq. (1), using the signal in the i th ring $\Delta S_i(\theta)$ and the ring's solid angle $\Delta\Omega_i$. For charge-transfer measurements, two data arrays are collected, one with gas in the TC and the other with no gas present, and two corresponding sets of ring counts are determined, denoted by $[\Delta S(\theta)]^{\text{in}}$ and $[\Delta S(\theta)]^{\text{out}}$, respectively. The signal $\Delta S(\theta)$ is calculated from the difference $[\Delta S(\theta)]^{\text{in}} - [\Delta S(\theta)]^{\text{out}}$. This procedure distinguishes counts due to scattering by the target gas from counts arising from extraneous sources.

Measurements of direct scattering require a different procedure since neutral products of charge transfer strike the detector along with scattered and unscattered ions. Collection of four data arrays is necessary to remove counts due to charge transfer and obtain the scattered ion signal. The $[\Delta S(\theta)]^{\text{in}}$ and $[\Delta S(\theta)]^{\text{out}}$ sets are taken as before. The $[\Delta S(\theta)]^{\text{in}}$ set in this case contains counts due to four contributions: (1) primary ion beam, (2) directly scattered ions, (3) neutral atoms from charge transfer, and (4) background counts; while the $[\Delta S(\theta)]^{\text{out}}$ set contains counts due to contributions (1) and (4). An additional data set $[\Delta S(\theta)]^{\text{ct}}$ is taken with gas in the target cell and DP activated so that only neutral particles strike the detector; $[\Delta S(\theta)]^{\text{ct}}$ contains counts due to (3) and (4). A further set of background $[\Delta S(\theta)]^{\text{bg}}$ is collected, containing only counts due to contribution (4). The direct scattering signal is then given as

$$\Delta S(\theta) = \{ [\Delta S(\theta)]^{\text{in}} + [\Delta S(\theta)]^{\text{bg}} \} - \{ [\Delta S(\theta)]^{\text{out}} + [\Delta S(\theta)]^{\text{ct}} \}. \quad (2)$$

The experimental uncertainty in the number of counts at a particular angle is primarily statistical, and ranges from 1% near 0.02° to 10% near 1° . The angular uncertainty arises from the finite width of the primary ion beam, the discrete width of the analysis rings, and electronic errors in the detector's position encoding circuits.

The collective uncertainty amounts to about 0.03° at the smallest scattering angles.

For charge-transfer measurements, the scattered flux $\Delta S(\theta)$ consists of neutral particles, whereas the primary flux S is ionic. The ions and atoms may be detected with different efficiencies, leading to cross sections whose absolute scale is not well determined. This issue has been considered previously¹⁰ with the conclusion that at 5.0 keV the two detection efficiencies are equal. However, a series of independent measurements of the H^+ -Kr charge-transfer cross section using four different PSD's has resulted in integrated cross sections (0° - 1.0°) varying by $\pm 5\%$ at 1.5 keV and $\pm 10\%$ at 0.5 keV. No systematic effects were observed, although a variety of configurations (PSD size 4.0 cm diameter versus 2.5 cm diameter; microchannel plate age, history, and manufactured quality) were used. The only apparent explanation for this result is that at these energies, the ratio of the ion and neutral detection efficiencies may vary slightly from one PSD to another. Therefore the present differential cross sections for charge transfer at 1.5 and 0.5 keV are subject to minimum additional $\pm 5\%$ and $\pm 10\%$ uncertainties, respectively. Even though the relative detection efficiencies of ions and neutral atoms may vary slightly from detector to detector, individual detectors exhibit uniform efficiency for ion detection over their entire surfaces.

TABLE I. Values of the differential cross sections in $\text{\AA}^2/\text{sr}$ at the indicated laboratory angles. The statistical uncertainty in the values is 5% at 0.1° and 10% at 0.8° . The letter D denotes direct scattering and CT denotes charge transfer.

Process	$\frac{d\sigma(\theta=0.1^\circ)}{d\Omega}$	$\frac{d\sigma(\theta=0.8^\circ)}{d\Omega}$
H^+ -Ne		
1.5 keV (D)	2.1×10^5	3.1×10^2
H^+ -Ar		
1.5 keV (D)	3.7×10^5	5.5×10^2
0.5 keV (CT)	3.7×10^4	8.4×10^2
1.5 keV (CT)	1.5×10^5	2.9×10^2
5.0 keV (CT)	1.8×10^5	4.4×10^2
H^+ -Kr		
1.5 keV (D)	2.9×10^5	5.3×10^2
0.5 keV (CT)	4.0×10^5	5.6×10^3
1.5 keV (CT)	2.9×10^5	6.9×10^2
5.0 keV CT	2.2×10^5	5.2×10^2
H^+ -Xe		
1.5 keV (D)	3.5×10^5	4.8×10^2
5.0 keV (CT)	1.5×10^5	5.1×10^2
He^+ -Ne		
1.5 keV (D)	1.7×10^5	1.8×10^3
1.5 keV (CT)	3.4×10^4	2.9×10^2
He^+ -Ar		
1.5 keV (D)	1.8×10^5	1.4×10^3
He^+ -Kr		
1.5 keV (D)	1.8×10^5	8.7×10^2
He^+ -Xe		
1.5 keV (D)	8.2×10^4	2.9×10^2

III. RESULTS AND DISCUSSION

Differential cross sections for direct scattering and charge transfer are shown in Figs. 2–7. In addition, the present absolute differential cross sections are given in Table I at 0.1° and 0.8° . Many effects contribute to the observed structure. Classical trajectory-dependent effects (such as rainbow scattering) contribute, as do quantum diffraction undulations (arising in scattering from a steeply rising repulsive potential wall). Trajectory effects have been observed in this laboratory in H^+ -He direct scattering cross sections,¹¹ and diffraction undulations were seen in neutral atom-atom scattering cross sections,⁹ where the interaction potential is almost completely repulsive. Processes in which more than one potential is involved in the collision often exhibit cross sections with a characteristic oscillatory behavior. These have been treated by so-called curve-crossing models, wherein transitions between the initial and final states occur over a localized range of internuclear separation as the reactants approach or recede from each other. Interference between the resulting scattering amplitudes is responsible for oscillations in the differential cross sections.

In the case of H^+ -rare-gas direct scattering, Abignoli *et al.*⁴ measured differential cross sections at comparable energies to those presented here but at larger angles, and their data included measurements of the energy loss of the protons. They reported that for H^+ -Ne, inelastic events are an order of magnitude less likely than elastic events at a reduced scattering angle of $\tau=1.6$ keV deg; and for H^+ -Ar direct scattering, although inelastic events (primarily excitation of the target *via* the lowest H-Ar⁺ state) are more frequent than in H^+ -Ne, the direct cross section below 1.0 keV deg is dominated by elastic events. This suggests that the structure in the corresponding present data for H^+ -Ne and H^+ -Ar (Fig. 2) arises from single-potential effects. For H^+ -Kr direct scattering, Abignoli reported that the inelastic cross section is comparable to the elastic cross section near 1 keV deg; while for H^+ -Xe direct scattering, inelastic events are even more important. Inelastic events may therefore contribute to the structure in the present H^+ -Kr cross sections shown in Fig. 2 (since these data include inelastic and elastic events). The large, regular oscillations in the present H^+ -Xe direct cross sections (Fig. 2) indicate that more than one potential contributes to the scattering, and are consistent with a regular oscillation observed by Abignoli in the charge-transfer probability at 0.5 keV. This reaction was studied by Kubach *et al.*,⁶ who observed and modeled the near-resonant charge transfer into the $Xe^+(^2P_{1/2,3/2})$ fine-structure states ($\Delta E = -0.17, -1.5$ eV for the $J = \frac{1}{2}, \frac{3}{2}$ states, respectively). Since the $H(1s)-Xe(^2P)$ potentials cross the $H^+-Xe(^1S_0)$ potential, Kubach used the Landau-Zener-Stueckelberg (LZS) model⁸ in a quantal calculation. The present 5.0-keV charge-transfer results (Fig. 3) show little structure, and one possible explanation is that at this higher energy other inelastic channels open. The correspondingly larger number of scattering amplitudes would result in more interference terms and tend to reduce the structure in the cross section. Charge-transfer

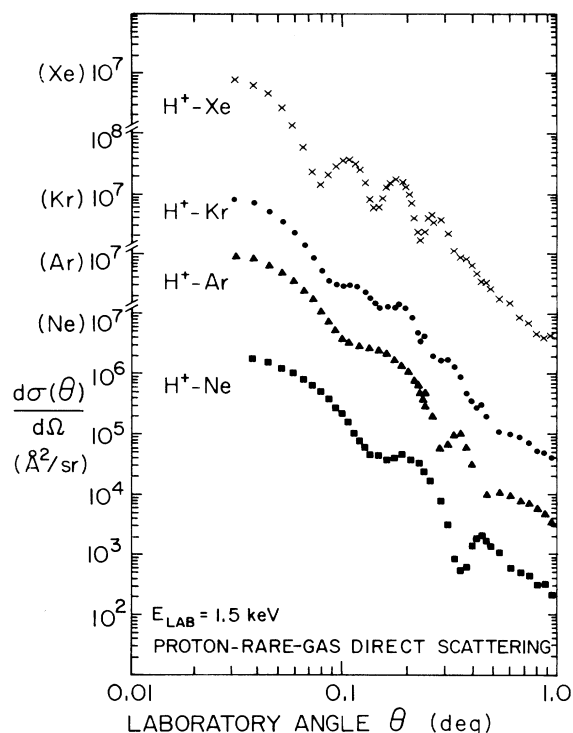


FIG. 2. Differential cross sections for direct scattering of H^+ -Ne, Ar, Kr, and Xe at a projectile energy of 1.5 keV. Note the shift of the y axis.

differential cross sections for H^+ -Ar and H^+ -Kr were also measured at comparable energies at larger angles by Abignoli *et al.*⁴ The regular oscillations in the present charge-transfer measurements (Figs. 4 and 5) are consistent with oscillations in charge-transfer cross sections

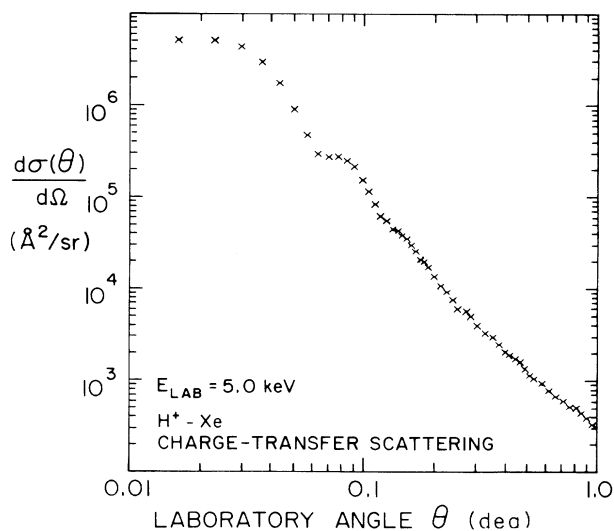


FIG. 3. Differential cross sections for direct and charge-transfer scattering of H^+ -Xe at a projectile energy of 5.0 keV.

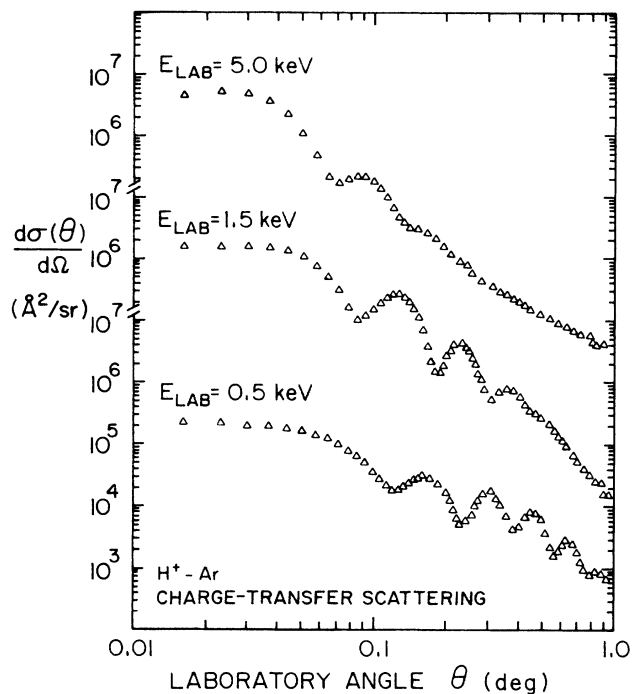


FIG. 4. Differential cross sections for charge-transfer scattering of H^+ -Ar at projectile energies of 0.5, 1.5, and 5.0 keV. Note the shift of the y axis.

observed by Abignoli. These processes have been modeled using Demkov transitions⁸ by Sidis¹³ and by Benoit *et al.*⁷

For He^+ -Ne direct scattering, Barat *et al.*⁵ observed that elastic processes exceed the largest inelastic effect

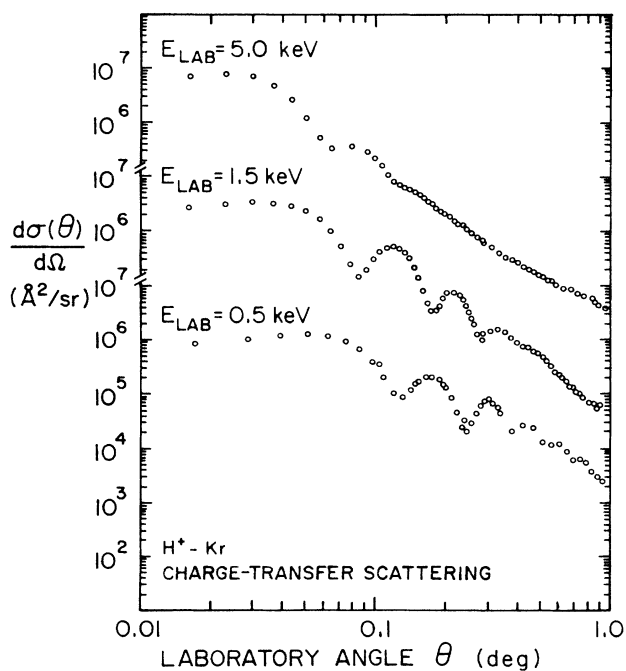


FIG. 5. Differential cross sections for charge-transfer scattering of H^+ -Kr at projectile energies of 0.5, 1.5, and 5.0 keV. Note the shift of the y axis.

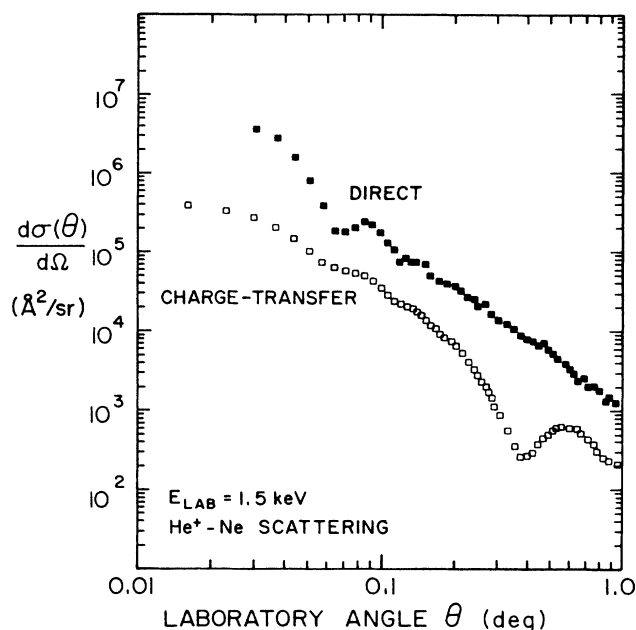


FIG. 6. Differential cross sections for direct and charge-transfer scattering of He^+ -Ne at a projectile energy of 1.5 keV.

[excitation of $Ne^*(2p^53s)$] by a factor of 5 at 1.5 keV and 1° scattering angle, indicating that the present results (Fig. 6) are dominated by elastic events. This reaction has also been investigated by Aberth and Lorents¹ and Helbig and Everhart.¹⁴ Direct scattering of He^+ -Ne has also been modeled extensively^{2,3,5,15-18} for both elastic

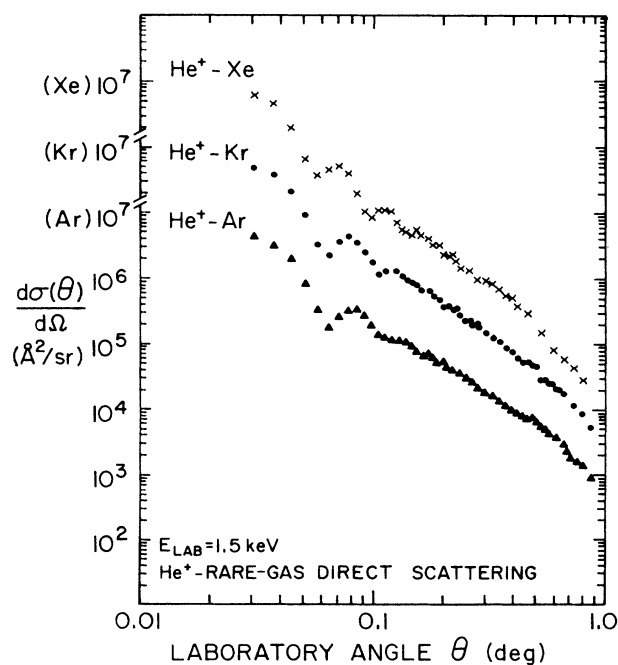


FIG. 7. Differential cross sections for direct scattering of He^+ -Ar, Kr, and Xe at a projectile energy of 1.5 keV. Note the shift of the y axis.

TABLE II. Absolute integral cross sections in \AA^2 , where the range of integration is also shown. The letter *D* denotes direct scattering and CT denotes charge transfer.

Process	Integration range	Integrated σ	Published total σ
H⁺-Ne			
1.5 keV (<i>D</i>)	$0.04^\circ \leq \theta \leq 1.0^\circ$	8.2	
H⁺-Ar			
1.5 keV (<i>D</i>)	$0.04^\circ \leq \theta \leq 1.0^\circ$	25.0	
0.5 keV (CT)	$0^\circ \leq \theta \leq 1.0^\circ$	4.4	5.0 ^a , 4.5 ^b , 5.0 ^c
1.5 keV (CT)	$0^\circ \leq \theta \leq 1.0^\circ$	11.0	14.0 ^a , 10.0 ^b
5.0 keV (CT)	$0^\circ \leq \theta \leq 1.0^\circ$	11.2	12.0 ^a , 15.0 ^d , 13.0 ^e , 17.4 ^f
H⁺-Kr			
1.5 keV (<i>D</i>)	$0.04^\circ \leq \theta \leq 1.0^\circ$	18.0	
0.5 keV (CT)	$0^\circ \leq \theta \leq 1.0^\circ$	25.0	26.0 ^a , 27.0 ^b , 31.0 ^c
1.5 keV (CT)	$0^\circ \leq \theta \leq 1.0^\circ$	20.0	25.0 ^a , 22.0 ^b
5.0 keV (CT)	$0^\circ \leq \theta \leq 1.0^\circ$	15.6	20.0 ^a , 20.0 ^d , 14.4 ^f
H⁺-Xe			
1.5 keV (<i>D</i>)	$0.04^\circ \leq \theta \leq 1.0^\circ$	14.4	
5.0 keV (CT)	$0^\circ \leq \theta \leq 1.0^\circ$	11.3	23.0 ^a , 20.0 ^d
He⁺-Ne			
1.5 keV (<i>D</i>)	$0.04^\circ \leq \theta \leq 1.0^\circ$	9.0	
1.5 keV (CT)	$0^\circ \leq \theta \leq 1.0^\circ$	1.8	1.5 ^a
He⁺-Ar			
1.5 keV (<i>D</i>)	$0.04^\circ \leq \theta \leq 1.0^\circ$	10.5	
He⁺-Kr			
1.5 keV (<i>D</i>)	$0.04^\circ \leq \theta \leq 1.0^\circ$	9.5	
He⁺-Xe			
1.5 keV (<i>D</i>)	$0.04^\circ \leq \theta \leq 1.0^\circ$	7.0	

^aStedeford and Hasted (Ref. 19).

^bLatypov and Shaporenko (Ref. 20).

^cKoopman (Ref. 21).

^dAfrimosov *et al.* (Ref. 22).

^eStier and Barnett (Ref. 23).

^fRudd *et al.* (Ref. 24).

events and inelastic events, which proceed *via* an LZS crossing transition. Barat observed a strongly oscillating charge-transfer cross section; a minimum is apparent in the present results (Fig. 6), which may be the beginning of an oscillatory pattern. Direct scattering for the remaining collision pairs He⁺-Ar, He⁺-Kr, and He⁺-Xe was studied by the SRI group^{1,2} and at comparable energies but larger angles by Baudon, Barat, and Abignoli. Their data indicate that although inelastic effects are important for large angles at keV energies, elastic processes dominate at sufficiently small angles (in the vicinity of 1° at keV energies), suggesting that the present cross sections (Fig. 7) are composed primarily of elastic events. The gentle undulations observed in the present data imply that an adequate description of the collision is possible using a single, repulsive potential.

The measured differential cross sections have been integrated over the observed angular range and are present-

ed in Table I. As has been observed in previous studies,^{10,11} ion-atom differential cross sections are strongly peaked in the forward direction and a large fraction of the total cross section is thus contained in the angular range below 1°. While it is not possible to reliably extrapolate the present data to larger angles for the purposes of determining total cross sections, it is illustrative to compare in Table II the present integral cross sections with total cross sections determined elsewhere.

ACKNOWLEDGMENTS

This work was supported by the Robert A. Welch Foundation, NASA, and the National Science Foundation, Atmospheric Sciences Section.

- ¹W. Aberth and D. C. Lorents, *Phys. Rev.* **144**, 109 (1966).
- ²F. T. Smith, R. P. Marchi, W. Aberth, D. C. Lorents, and O. Heinz, *Phys. Rev.* **161**, 31 (1967).
- ³J. Baudon, M. Barat, and M. Abignoli, *J. Phys. B* **3**, 207 (1970).
- ⁴M. Abignoli, M. Barat, J. Baudon, J. Fayeton, and J. C. Houver, *J. Phys. B* **5**, 1533 (1972).
- ⁵M. Barat, J. C. Brenot, D. Dhuicq, J. Pommier, V. Sidis, R. E. Olson, E. J. Shipsey, and J. C. Browne, *J. Phys. B* **9**, 269 (1976).
- ⁶C. Kubach, C. Benoit, V. Sidis, J. Pommier, and M. Barat, *J. Phys. B* **9**, 2073 (1976).
- ⁷C. Benoit, C. Kubach, V. Sidis, J. Pommier, and M. Barat, *J. Phys. B* **10**, 1661 (1977).
- ⁸L. D. Landau, *Z. Phys. Sov. Union* **2**, 46 (1932); C. Zener, *Proc. R. Soc. London Ser. A* **137**, 696 (1932); E. C. G. Stueckelberg, *Helv. Phys. Acta* **5**, 370 (1932); Y. N. Demkov, *Zh. Eksp. Teor. Fiz.* **45**, 195 (1963) [*Sov. Phys.—JETP* **18**, 138 (1964)].
- ⁹D. E. Nitz, R. S. Gao, L. K. Johnson, K. A. Smith, and R. F. Stebbings, *Phys. Rev. A* **35**, 4541 (1987); R. S. Gao, L. K. Johnson, D. E. Nitz, K. A. Smith, and R. F. Stebbings, *ibid.* **36**, 3077 (1987); L. K. Johnson, R. S. Gao, K. A. Smith, and R. F. Stebbings, *ibid.* **38**, 2794 (1988).
- ¹⁰R. S. Gao, L. K. Johnson, J. H. Newman, K. A. Smith, and R. F. Stebbings, *Phys. Rev. A* **38**, 2789 (1988).
- ¹¹L. K. Johnson, M. Kimura, R. S. Gao, K. A. Smith, N. F. Lane, and R. F. Stebbings (unpublished).
- ¹²J. H. Newman, K. A. Smith, R. F. Stebbings, and Y. S. Chen, *J. Geophys. Res.* **90**, 11045 (1985); J. H. Newman, Y. S. Chen, K. A. Smith, and R. F. Stebbings, *ibid.* **91**, 8947 (1986).
- ¹³V. Sidis, *J. Phys. B* **5**, 1517 (1972).
- ¹⁴H. F. Helbig and E. Everhart, *Phys. Rev.* **136**, A674 (1964).
- ¹⁵P. R. Jones, F. P. Ziemba, H. A. Moses, and E. Everhart, *Phys. Rev.* **113**, 182 (1959); E. N. Fuls, P. R. Jones, F. P. Ziemba, and E. Everhart, *ibid.* **107**, 704 (1957).
- ¹⁶V. Sidis and H. Lefebvre-Brion, *J. Phys. B* **4**, 1040 (1971).
- ¹⁷S. M. Bobbio, L. D. Doverspike, and R. L. Champion, *Phys. Rev. A* **7**, 526 (1973).
- ¹⁸R. E. Olson and F. T. Smith, *Phys. Rev. A* **3**, 1607 (1971); D. Coffey, D. C. Lorents, and F. T. Smith, *Phys. Rev.* **187**, 201 (1969).
- ¹⁹J. B. H. Stedeford and J. B. Hasted, *Proc. R. Soc. London Ser. A* **227**, 406 (1955).
- ²⁰Z. Z. Latypov and A. A. Shaporenko, *Zh. Tekh. Fiz.* **46**, 1277 (1976).
- ²¹D. W. Koopman, *Phys. Rev.* **154**, 79 (1967).
- ²²V. V. Afrimosov, Y. A. Mamaev, M. N. Panov, V. Uroshevich, and N. V. Fedorenko, *Zh. Tekh. Fiz.* **37**, 550 (1967) [*Sov. Phys. Tech. Phys.* **12**, 394 (1967)]; V. V. Afrimosov, Y. A. Mamaev, M. N. Panov, and N. V. Fedorenko, *ibid.* **39**, 159 (1969) [*ibid.* **14**, 109 (1969)].
- ²³P. M. Stier and C. F. Barnett, *Phys. Rev.* **103**, 896 (1956).
- ²⁴M. E. Rudd, R. D. DuBois, L. H. Toburen, C. A. Ratcliffe, and T. V. Goffe, *Phys. Rev. A* **28**, 3244 (1983).